

Cosmic ray driven dynamo in galactic disks. A parameter study

Michał Hanasz¹, Katarzyna Otmianowska-Mazur², Grzegorz Kowal^{2,3}, Harald Lesch⁴

¹ Toruń Centre for Astronomy, Nicolaus Copernicus University, PL-87-148 Toruń/Piwnice, Poland

² Astronomical Observatory, Jagiellonian University, ul. Orła 171, 30-244 Kraków

³ Department of Physics and Astronomy, McMaster University, 1280 Main St. W., Hamilton, ON L8S 4M1, Canada

⁴ Astronomical Observatory, Munich University, Scheinerstr. 1, D-81679, Germany

Received ...; accepted ...

ABSTRACT

Aims. We present a parameter study of the magnetohydrodynamical dynamo driven by cosmic rays in the interstellar medium (ISM) focusing on the efficiency of magnetic field amplification and the issue of energy equipartition between magnetic, kinetic and cosmic ray (CR) energies.

Methods. We perform numerical CR-MHD simulations of the ISM using the extended version of ZEUS-3D code in the shearing box approximation and taking into account the presence of Ohmic resistivity, tidal forces and vertical disk gravity. CRs are supplied in randomly distributed supernova (SN) remnants and are described by the diffusion-advection equation, which incorporates an anisotropic diffusion tensor.

Results. The azimuthal magnetic flux and total magnetic energy are amplified in majority of models depending on a particular choice of model parameters. We find that the most favorable conditions for magnetic field amplification correspond to magnetic diffusivity of the order of $3 \times 10^{25} \text{ cm}^2 \text{ s}^{-1}$, SN rates close to those observed in the Milky Way, periodic SN activity corresponding to spiral arms, and highly anisotropic and field-aligned CR diffusion. The rate of magnetic field amplification is relatively insensitive to the magnitude of SN rates in a range of spanning 10% up to 100% of realistic values. The timescale of magnetic field amplification in the most favorable conditions is 150 Myr, at galactocentric radius equal to 5 kpc, which is close to the timescale of galactic rotation. The final magnetic field energies reached in the efficient amplification cases fluctuate near equipartition with the gas kinetic energy. In all models CR energy exceeds the equipartition values by a least an order of magnitude, in contrary to the commonly expected equipartition. We suggest that the excess of cosmic rays in numerical models can be attributed to the fact that the shearing-box does not permit cosmic rays to leave the system along the horizontal magnetic field, as it may be the case of real galaxies.

Key words. Galaxies: ISM - magnetic fields - ISM: cosmic rays - magnetic fields - kinematics and dynamics - MHD

1. Introduction

An attractive idea of *fast galactic dynamo* has been proposed by Parker (1992). The idea relies on two ingredients: (1) cosmic rays (CR) continuously supplied to the disk by supernova (SN) remnants and (2) fast magnetic reconnection which operates in current sheets and allows to dissipate and relax the random magnetic field components in the limit of vanishing resistivity. Over the last decade we have investigated the different elements, physical properties and consequences of Parker's idea and scenario by means of analytical calculations and numerical simulations (Hanasz & Lesch 1993, 1997, 1998, 2000, 2001, 2003a, 2003b, Hanasz et al. 2002, 2004, 2006, Lesch & Hanasz 2003; Otmianowska-Mazur et al. 2003, 2007; Kowal et al. 2003, 2005)

The first complete 3D numerical model of the CR-driven dynamo has been demonstrated by Hanasz et al. (2004, 2006). In this paper we perform a parameter study of the CR-driven dynamo model by examining the dependence of magnetic field amplification on magnetic diffusivity, supernova rate determining the CR injection rate, temporal modulation of SN activity, grid resolution, and CR diffusion coefficients.

The principle of action of the CR-driven dynamo is based on the cosmic ray energy supplied continuously by SN remnants. Due to the anisotropic diffusion of cosmic rays and the horizontal magnetic field configuration, cosmic rays tend to accumulate within the disc volume. However, the configuration stratified by vertical gravity is unstable with respect to the Parker instability. Buoyancy effects induce vertical and horizontal motions of the fluid and formation of undulated patterns – magnetic loops in frozen-in, predominantly horizontal magnetic fields. The presence of rotation in galactic disks implies a coherent twisting of the loops by means of the Coriolis force, which leads to the generation of small-scale radial magnetic field components. The next phase is merging of small-scale loops by the magnetic reconnection process to form the large scale radial magnetic fields. Finally, the differential rotation stretches the radial magnetic field to amplify the large-scale azimuthal magnetic field component. The coupling of amplification processes of radial and azimuthal magnetic field components results in an exponential growth of the large scale magnetic field. The timescale of magnetic field amplification, resulting from the action of the CR-driven dynamo, has been found (Hanasz et al. 2004, 2006) to be equal to 140- 250 Myr, depending on the galactocentric radius, which is comparable to the galactic rotation period.

The CR-dynamo experiments reported in the afore mentioned papers rely on energy of CRs accelerated in SN remnants. Recently Gressel et al. (2008a,b) reported a series of non-ideal MHD simulations demonstrating dynamo action resulting from the SN-driven turbulence, in absence of CRs. Using a similar set of galactic disk parameters, with angular velocity enlarged 4 times the value of 0.025Myr^{-1} , typical for the galactocentric radius of Sun, these authors found amplification of the large scale magnetic fields on a time scale of 250Myr . This indicates some similarity between the CR-driven dynamo and the dynamo driven by thermal energy output from supernovae. The similarity is presumably related to the buoyancy effect which can be commonly attributed to the excess of both the thermal and cosmic ray energies in the disk volume.

The magnitudes of galactic magnetic fields are usually estimated from measurements of the radio synchrotron emission arising from the acceleration of cosmic ray electrons in the magnetic field. To interpret the radio emission spectrum, it is usually assumed that the energy density in the magnetic field is of the same order of magnitude as the energy density in cosmic ray protons (which are assumed to outnumber the electrons by 100:1, as they do in our Galaxy). There is however no compelling evidence of energy equipartition. Since the equipartition or minimum energy assumption is one of the few ways to calculate radio source parameters, it is important to determine how reasonable the approach generally is. Recently Strong et al. (2007) and Snodin et al. (2005) raised again the question about the applicability of the equipartition argument.

From the observational point of view (Fitt and Alexander 1993; Vallee 1995) the equipartition assumption seems to hold. In particular, Vallee's comparison of three different methods determining galactic magnetic field strengths (Faraday rotation method, equipartition method and Cosmic ray equipartition) shows that the equipartition fields are in a quite good agreement. On the other hand, Beck and Krause (2005) considered in detail a problem which was raised by Chi and Wolfendale (1993), that the commonly used classical equipartition or minimum-energy estimate of total magnetic field strengths from radio synchrotron intensities is of limited practical use because it is based on the hardly known ratio K of the total energies of cosmic ray protons and electrons and also has inherent problems. They present a revised formula using the number density ratio K for which they give estimates. For particle acceleration in strong shocks K is about 40 and increases with decreasing shock strength. Their revised estimate for the field strength gives larger values than the classical estimate for flat radio spectra with spectral indices of about 0.5-0.6, but smaller values for steep spectra and total fields stronger than about $10\ \mu\text{G}$. In very young supernova remnants, for example, the classical estimate may be too large by up to 10. On the other hand, if energy losses of cosmic ray electrons are important, K increases with particle energy and the equipartition field may be underestimated significantly.

From a more global point of view the assumption of equipartition seems to be a very natural one. A thermodynamical system will always distribute the free energy to all degrees of freedom available, if the system has time to do so. In cases of accelerated particles diffusing in the large-scale and turbulent magnetic fields one can expect that at least the turbulent magnetic field (since it represents three degrees of freedom) is somehow virialized with respect to any other pressure term, like the cosmic ray pressure. This may not be true for the ordered magnetic fields, which are supposed to be amplified by the combined action of differentially rotating shear flows in the disk and some helical upward and downward motion driven either by cosmic rays pres-

sure or any activity in the disk. In any case the connection of star formation activity accompanied by enhanced flux of cosmic rays and the amplification of large-scale magnetic fields, inherently raises the expectation that magnetic fields should not exhibit higher pressures than the cosmic rays. Moreover, one would rather expect to find magnetic fields whose pressure is somewhat lower than the pressure of the cosmic rays, if the cosmic rays present a source for the galactic dynamo.

The paper is organized as follows: in Sect. 2 we describe the CR driven dynamo model and its numerical implementation, in Sect. 3 we present our simulation setup and describe parameters used in numerical simulations, in Sect. 4 we describe results, focusing on the effect of each parameter on magnetic field amplification rate. We discuss the final saturated states of models in terms of equipartition between kinetic, magnetic and CR energies. Finally, in Sect. 5 we conclude our paper.

2. Description of the model

Similarly as in the papers by Hanasz et al (2004, 2006) we take into account the following elements of the CR-driven dynamo:

- (1) The cosmic ray component, a relativistic gas, which is described by the diffusion-advection transport equation (see Hanasz & Lesch 2003b for the details of numerical algorithm). The typical values of the diffusion coefficient found from fitting to CR data (see eg. Strong et al 2007) are $(3 \div 5) \times 10^{28} \text{cm}^2 \text{s}^{-1}$ at energies $\sim 1\text{GeV}$, and even larger values $10^{29} \text{cm}^2 \text{s}^{-1}$ are mentioned (Jokipii 1999), however, we shall use reduced values in majority of simulations.
- (2) Following Giacalone & Jokipii (1999) and Jokipii (1999) we presume that cosmic rays diffuse anisotropically along magnetic field lines. The ratio of the perpendicular to parallel CR diffusion coefficients suggested by these authors is 5 %.
- (3) Localized sources of cosmic rays: supernova remnants exploding randomly in the disk volume (see Hanasz & Lesch 2004). We assume that each SN remnant supplies cosmic rays almost instantaneously, i.e. the cosmic ray input equal to 10 % of the canonical SN kinetic energy output ($= 10^{51} \text{erg}$) for a single SN remnant is distributed over several subsequent time-steps.
- (4) Resistivity of the ISM (see Hanasz et al. 2002, Hanasz & Lesch 2003a, Tanuma et al. 2003) responsible for the onset of fast magnetic reconnection and topological evolution of magnetic field lines. In this paper we apply the uniform resistivity and neglect the Ohmic heating of gas by resistive dissipation of magnetic fields.
- (5) Shearing boundary conditions and tidal forces following the prescription by Hawley, Gammie & Balbus (1995) aimed to model differentially rotating disks in the local approximation.
- (6) Realistic vertical disk gravity following the model of ISM in the Milky Way by Ferriere (1998).

The set of equations describing the model of the CR-driven dynamo includes resistive MHD and the cosmic ray transport equations (see Hanasz et al., 2004):

$$\frac{\partial \rho}{\partial t} + \nabla \cdot (\rho \mathbf{V}) = 0, \quad (1)$$

$$\frac{\partial e}{\partial t} + \nabla \cdot (e \mathbf{V}) = -p (\nabla \cdot \mathbf{V}), \quad (2)$$

$$\begin{aligned} \frac{\partial \mathbf{V}}{\partial t} + (\mathbf{V} \cdot \nabla) \mathbf{V} = & -\frac{1}{\rho} \nabla \left(p + p_{\text{cr}} + \frac{B^2}{8\pi} \right) \\ & + \frac{\mathbf{B} \cdot \nabla \mathbf{B}}{4\pi\rho} - 2\boldsymbol{\Omega} \times \mathbf{v} + 2q\Omega^2 x \hat{\mathbf{e}}_x + g_z(z) \hat{\mathbf{e}}_z, \end{aligned} \quad (3)$$

$$\frac{\partial \mathbf{B}}{\partial t} = \nabla \times (\mathbf{V} \times \mathbf{B}) + \eta \Delta \mathbf{B}, \quad (4)$$

$$p = (\gamma - 1)e, \quad \gamma = 5/3 \quad (5)$$

where $q = -d \ln \Omega / d \ln R$ is the shearing parameter, R is the distance to galactic center, η is the resistivity, γ is the adiabatic index of thermal gas, the gradient of cosmic ray pressure ∇p_{cr} is included in the equation of motion (see eg. Berezhinski et al. 1990) and other symbols have their usual meaning. The uniform resistivity is included only in the induction equation (see Hanasz et al. 2002). The thermal gas component is currently treated as an adiabatic medium.

The transport of the cosmic ray component is described by the diffusion-advection equation (see eg. Berezhinski et al. 1990, Schlickeiser & Lerche 1985)

$$\frac{\partial e_{cr}}{\partial t} + \nabla \cdot (e_{cr} \mathbf{V}) = \nabla \cdot (\hat{K} \nabla e_{cr}) - p_{cr} (\nabla \cdot \mathbf{V}) + Q_{SN}, \quad (6)$$

where Q_{SN} represents the source term for the cosmic ray energy density: the rate of production of cosmic rays injected locally in the SN remnants and

$$p_{cr} = (\gamma_{cr} - 1)e_{cr}, \quad \gamma_{cr} = 14/9. \quad (7)$$

The adiabatic index of the cosmic ray gas γ_{cr} and the formula for diffusion tensor

$$K_{ij} = K_{\perp} \delta_{ij} + (K_{\parallel} - K_{\perp}) n_i n_j, \quad n_i = B_i / B, \quad (8)$$

are adopted following the argumentation by Ryu et al. (2003).

3. Numerical simulations

3.1. Simulation setup

In this paper we present a series of recent numerical simulations, whose aim is to search for the most favorable conditions for magnetic field amplification by means of the CR-driven dynamo. The presented numerical simulations were performed with the aid of Zeus-3D MHD code (Stone and Norman 1992 a,b) extended with additions to the standard algorithm, that correspond to items (1) - (6) of Sect. 2, i.e. the cosmic ray component, treated as a fluid and described by the diffusion-advection equation, including anisotropic CR diffusion tensor and cosmic ray sources – supernova remnants exploding randomly in the disk volume, resistivity of the ISM leading to magnetic reconnection, shearing-periodic boundary conditions, rotational pseudo-forces and a realistic vertical disk gravity.

All simulations are performed in a Cartesian domain of size $0.5 \text{ kpc} \times 1 \text{ kpc} \times 2 \text{ kpc}$ in x , y , z coordinates, corresponding to radial, azimuthal and vertical directions, respectively. The basic resolution of the numerical grid is $50 \times 100 \times 400$ grid cells in x , y and z directions, respectively, and for a smaller sample of simulations performed with larger values of CR diffusion coefficients the grid resolution is $25 \times 50 \times 200$ grid cells. The boundary conditions are sheared-periodic in coordinate x , periodic in coordinate y and outflow on outer z -boundaries, with $e_{cr} = 0$ at the domain boundaries. The positions of SN are chosen randomly, with a uniform distribution in xy coordinates and Gaussian distribution in z coordinate.

The initial density distribution results from integration of the hydrostatic equilibrium equation, for the vertical gravity model of Ferriere (1998) and with the assumption of constant gas temperature across the disk, equal approximately 6000 K corresponding to the sound speed equal to about 7 km/s. The integration procedure finds hydrostatic equilibrium for a given gas column density treated as an input parameter.

The magnetic field strength, incorporated in the initial hydrostatic equilibrium of gas, is defined through the parameter α denoting the ratio of initial magnetic to gas pressures. The initial cosmic ray pressure is equal to the initial gas pressure.

The CR energy supplied to the system in SN remnants, randomly distributed around the disk midplane, implies that the CR pressure gradient force accelerates a vertical wind of thermal gas. To prevent significant mass losses from the computational domain, due to the vertical wind, we compensate the mass-loss Δm after each timestep. The compensation mass is supplied as a mass source term, which is proportional to the initial mass distribution

$$\Delta \rho(x, y, z) = \frac{\Delta m}{m_{\text{tot}}} \rho_0(x, y, z), \quad (9)$$

where m_{tot} is the total gas mass in the computational domain and $\rho_0(x, y, z)$ is the initial density distribution, resulting from the integration procedure of the hydrostatic equilibrium equation.

3.2. Simulation parameters

The basic input parameters, resulting from the assumed model are: the vertical gravity profile, local value of the galactic rotation and shear, gas column density and supernova rate. We adopt these parameters from the global model of ISM in Milky Way (Ferriere 1998) for the galactocentric radius $R = 5 \text{ kpc}$, where angular velocity is $\Omega = 0.05 \text{ Myr}^{-1}$, gas column density $\Sigma = 27 \times 10^{20} \text{ cm}^{-2}$ and the realistic vertical gravity given by formula (36) in the aforementioned paper. The values of gas column density correspond in our simulations to the total density of all gas components in Ferriere (1998), while SN-rate is the rate of type II supernovae. We assume for simplicity that all SN explosions appear as single supernovae, and that vertical distribution of SN explosions is Gaussian, with a fixed half-width equal to 100 pc.

In addition to the mentioned relatively well established local disk parameters, there is a group of less known quantities like effective magnetic diffusivity, CR diffusion coefficients and efficiency of conversion of SN kinetic energy into cosmic ray energy. We assume the standard 10% value of kinetic CR energy conversion efficiency and the magnetic diffusivity and CR diffusion coefficients varying in a wide range.

In this paper we present the results of five simulation series A–E. The summary of all variable simulations parameters for the whole set of simulations is presented in Table 1.

In simulation series A (runs A1 - A5) we examine effects of magnetic diffusivity variations on magnetic field amplification by applying η in the range $0 \div 10^3 \text{ pc}^2 \text{ Myr}^{-1}$ corresponding to $0 \div 3 \times 10^{26} \text{ cm}^2 \text{ s}^{-1}$ in CGS units. We define the magnetic Reynolds number $Rm = L_y^2 \Omega / \eta$ for reference, as in Gressel et al. (2008b), where $L_y = 1000 \text{ pc}$ is the domain size in y direction. Moreover we assume continuous and time-invariable supply of CRs in SN remnants. The simulation runs A1, A2, A3 are the same as the runs B, C, and D, respectively, discussed by Otmianowska-Mazur et al (2007). We note, for comparison, that the commonly adopted value of turbulent diffusivity in the ISM is $\eta_{\text{turb}} \approx 1/3 v_{\text{turb}} L_{\text{turb}} \sim 10^{26} \text{ cm}^2 \text{ s}^{-1}$ ($\approx 1/3 \times 10^3 \text{ pc}^2 \text{ Myr}^{-1}$) for $v_{\text{turb}} = 10 \text{ km s}^{-1}$ and $L_{\text{turb}} = 100 \text{ pc}$. We note that the adopted values of magnetic diffusivity exceed the value corresponding to the Spitzer resistivity ($\approx 10^8 \text{ cm}^2 \text{ s}^{-1}$, see Parker 1992) by 15–18 orders of magnitude. The relative smallness of the Spitzer resistivity implies that an anomalous resistivity, considered as a subscale phenomenon, has to be invoked in order to explain

Simulation	α	η [pc ² Myr ⁻¹]	Rm	f_{SN} [kpc ⁻² Myr ⁻¹]	f_{SN} modul. (Y/N)	K_{\parallel} [pc ² Myr ⁻¹]	K_{\perp} [pc ² Myr ⁻¹]	$n_x \times n_y \times n_z$
A1	10 ⁻⁴	0	∞	130	N	1 × 10 ⁴	1 × 10 ³	100 × 50 × 400
A2	10 ⁻⁴	1	5 × 10 ⁴	130	N	1 × 10 ⁴	1 × 10 ³	100 × 50 × 400
A3	10 ⁻⁴	10	5 × 10 ³	130	N	1 × 10 ⁴	1 × 10 ³	100 × 50 × 400
A4	10 ⁻⁴	100	5 × 10 ²	130	N	1 × 10 ⁴	1 × 10 ³	100 × 50 × 400
A5	10 ⁻⁴	1000	5 × 10 ¹	130	N	1 × 10 ⁴	1 × 10 ³	100 × 50 × 400
B1	10 ⁻⁴	0	∞	130	Y	1 × 10 ⁴	1 × 10 ³	100 × 50 × 400
B2	10 ⁻⁴	1	5 × 10 ⁴	130	Y	1 × 10 ⁴	1 × 10 ³	100 × 50 × 400
B3	10 ⁻⁴	10	5 × 10 ³	130	Y	1 × 10 ⁴	1 × 10 ³	100 × 50 × 400
B4	10 ⁻⁴	100	5 × 10 ²	130	Y	1 × 10 ⁴	1 × 10 ³	100 × 50 × 400
B5	10 ⁻⁴	1000	5 × 10 ¹	130	Y	1 × 10 ⁴	1 × 10 ³	100 × 50 × 400
C1	10 ⁻⁴	100	5 × 10 ²	15	Y	1 × 10 ⁴	1 × 10 ³	100 × 50 × 400
C2	10 ⁻⁴	100	5 × 10 ²	30	Y	1 × 10 ⁴	1 × 10 ³	100 × 50 × 400
C3	10 ⁻⁴	100	5 × 10 ²	60	Y	1 × 10 ⁴	1 × 10 ³	100 × 50 × 400
C4	10 ⁻⁴	100	5 × 10 ²	250	Y	1 × 10 ⁴	1 × 10 ³	100 × 50 × 400
C5	10 ⁻⁴	100	5 × 10 ²	500	Y	1 × 10 ⁴	1 × 10 ³	100 × 50 × 400
D1	10 ⁻⁴	100	5 × 10 ²	130	N	1 × 10 ⁴	1 × 10 ³	50 × 25 × 200
D2	10 ⁻⁴	100	5 × 10 ²	130	Y	1 × 10 ⁴	1 × 10 ³	50 × 25 × 200
E1	10 ⁻²	100	5 × 10 ²	130	N	1 × 10 ⁴	3 × 10 ³	50 × 25 × 200
E2	10 ⁻²	100	5 × 10 ²	130	N	3 × 10 ⁴	1 × 10 ³	50 × 25 × 200
E3	10 ⁻²	100	5 × 10 ²	130	N	3 × 10 ⁴	3 × 10 ³	50 × 25 × 200
E4	10 ⁻²	100	5 × 10 ²	130	N	3 × 10 ⁴	1 × 10 ⁴	50 × 25 × 200
E5	10 ⁻²	100	5 × 10 ²	130	N	1 × 10 ⁵	1 × 10 ³	50 × 25 × 200
E6	10 ⁻²	100	5 × 10 ²	130	N	1 × 10 ⁵	3 × 10 ³	50 × 25 × 200
E7	10 ⁻²	100	5 × 10 ²	130	N	1 × 10 ⁵	1 × 10 ⁴	50 × 25 × 200

Table 1. Parameters of simulations presented in this paper. Subsequent columns show: simulation name, initial ratio of magnetic to gas pressure α , magnetic diffusivity η , magnetic Reynolds number Rm, surface frequency of SN explosions, presence of SN-rate modulation, parallel K_{\parallel} and perpendicular K_{\perp} CR diffusion coefficients, and grid resolution in x , y and z directions.

dissipation of the small scale magnetic fluctuations in the ISM. Following Parker (1992), we assume that reconnection rates in the ISM are comparable to those predicted by the Petscheck’s fast reconnection model, i.e. the magnetic cutting speeds are of the order of $v_A / \log(R_M)$ rather than $v_A / \sqrt{R_M}$ typical for the slow Parker-Sweet reconnection model, where R_M is the Lundquist number or the magnetic Reynolds number.

In the simulation series B (runs B1 - B5) we apply the same range of magnetic diffusivity values, but CRs supply is modulated in a manner mimicking passages of subsequent spiral arms, regulating the star formation rate and subsequently SN-rate. The effect of spiral arms is modelled (see Hanasz et al. 2006) by supplying cosmic rays in intermittent periods of 25 Myr, with SN rate equal to 4× the reference f_{SN} , and followed by periods of 75 Myr without any SN activity. The time-averaged supernova rate is in this case equal to the reference f_{SN} .

In the simulation series C (runs C1-C5) we apply a constant magnetic diffusivity $\eta = 100\text{pc}^2\text{Myr}^{-1}$ and vary the surface frequency of SN explosions in the range of 15 – 500 $\text{kpc}^{-2}\text{Myr}^{-1}$, assuming modulated CR supply as in the simulation series B. In the simulation series D (runs D1 - D2) we repeat simulations A4 and B4, respectively, with the grid resolution reduced twice in each spatial direction.

Due to the CFL timestep limitation of the currently used explicit algorithm of CR diffusion, the applied values of CR diffusion coefficients are scaled down with respect to the realistic values. The timestep limitation ensuring stability of explicit numerical schemes applied to the diffusion equation is $\Delta t \leq 0.5(\Delta x)^2/K$, where K is the diffusion coefficient. The timestep becomes prohibitively short when the diffusion coefficient is very large or the spatial step is too small. For this reason the CR diffusion coefficient has been reduced in simulation series A-D, by about one order of magnitudes, with respect to the mentioned realistic values $3 \div 6 \times 10^{28}\text{cm}^2\text{s}^{-1} \approx 1 \div 2 \cdot 10^5\text{pc}^2\text{Myr}^{-1}$. The fiducial values of the parallel and perpendicular diffusion coefficients applied in simulation series

A–D are respectively: $K_{\parallel} = 1 \times 10^4\text{pc}^2\text{Myr}^{-1} \approx 3 \times 10^{27}\text{cm}^2\text{s}^{-1}$ and $K_{\perp} = 1 \times 10^3 \approx 3 \times 10^{26}\text{cm}^2\text{s}^{-1}$.

Finally, in the simulation series E (runs E1 - E6) we increase the parallel K_{\parallel} and perpendicular K_{\perp} CR diffusion coefficients by factors 3 and 10, with respect to the fiducial values, in order to examine magnetic field amplification for more realistic magnitudes of these quantities. In this way we apply realistic CR diffusion coefficients in a few single simulation runs, yet the maximum CR diffusion coefficients used do not reach the upper range of realistic values, of the order of $10^{29}\text{cm}^2\text{s}^{-1}$, mentioned in the literature.

4. Results

In Fig. 1 we show the distribution of cosmic ray gas together with magnetic field vectors (panel (a)), and thermal gas density together with gas velocity vectors (panel (b)) in the yz -slice taken for $x = 0$ at $t = 1000$ Myr.

One can notice in panel (a) that the dominating horizontal magnetic field component in the disk volume is undulated in a manner resembling the effects of Parker instability. The cosmic ray energy density is well smoothed by the diffusive transport in the computational volume. The vertical gradient of the cosmic ray energy density is maintained by the supply of cosmic rays around the equatorial plane in the disk in the presence of vertical gravity. The cosmic ray energy density is expressed in units in which the thermal gas energy density corresponding to $\rho = 1\text{cm}^{-3}$ and the isothermal sound speed $c_s = 7\text{km s}^{-1}$ is equal to 1. The velocity field together with gas density is shown in panel (b). It is apparent that the distribution of gas is significantly less smooth than the distribution of cosmic rays.

In order to examine the structure of the large-scale field we show in panel (c) the horizontally averaged magnetic field components $\langle B_x(z) \rangle$ and $\langle B_y(z) \rangle$. A striking property of the mean magnetic field configuration is the almost exact coincidence of peaks of the oppositely directed radial and azimuthal field components. This feature resembles to the standard picture of an $\alpha\omega$ -

dynamo: the azimuthal mean magnetic component is generated from the radial one and vice versa (see Lesch and Hanasz (2003) for a corresponding simple analytical model).

In panel (d) we show the horizontally averaged vertical velocity component $\langle V_z \rangle$ and its fluctuations $\langle \delta V_z \rangle$. It is apparent that the bulk speeds of the wind, driven by the vertical gradient of CR pressure, reach $65 \pm 15 \text{ km/s}$ at $z = \pm 2 \text{ kpc}$. Vertical systematic winds blowing with bulk speeds, comparable to rotational galactic velocities, influence large-scale structures of galactic magnetic fields and are observed in external starburst galaxies like NGC 253 (see Beck 2007, Hesse et al. 2008).

By varying the parameters discussed in the previous section we intend to determine the regions of parameter space in which the magnetic field amplification is the most efficient. The amplification of the regular magnetic field is identified with the amplification of the total magnetic energy in the computational domain, associated with the amplification of the azimuthal magnetic flux. The magnetic flux shown in subsequent plots represents an azimuthal flux averaged over all xz slices (spread in y direction) through the discretized computational domain. In the subsequent subsections we present the parameter study of the CR-driven dynamo, focusing on the efficiency of magnetic field amplification and the issue of equipartition between magnetic, kinetic, and CR energies.

4.1. Dependence of magnetic field amplification on magnetic diffusivity

As a first step in our parameter study of the cosmic-ray driven dynamo we examine, in simulation series A, the effect of magnetic diffusivity on the efficiency of magnetic field amplification. Time evolution of magnetic energy and magnetic flux are shown in Fig. 2. Magnetic flux plotted in the left panel of Fig. 2 is scaled in the following way. The initial magnetic field induction is defined by the parameter $\alpha = p_{\text{mag}}/p_{\text{gas}}$, shown in the second column of Table. 1, where we apply Parker's convention to assign the inverse of plasma beta as α . The adopted values of α are 10^{-4} and 10^{-2} in different simulations, while $\alpha = 1$ means magnetic pressure equal to the thermal gas pressure. We scale magnetic flux in such a way that $\alpha = 1$ corresponds to the azimuthal magnetic flux $\Phi_a = 1$. The total magnetic energy plotted in the right panel of Fig. 2 is scaled with respect to the time-averaged total kinetic energy in the computational domain. The latter quantity appears to fluctuate around a mean value, which is practically time-invariant for all simulation runs, thus we find this kind of scaling convenient. The scaling described above will be applied to all subsequent plots of magnetic flux and magnetic energy.

The evolution of magnetic energy and magnetic flux in models of simulation series A, represented by different curves in Fig. 2, demonstrate that magnetic field amplification strongly depends on magnetic diffusivity. In the case of vanishing explicit resistivity, magnetic energy grows up by about 2.5 orders of magnitude during the first 500 Myr, but magnetic flux is amplified only by a factor of 3 during this period and it fades later on. This effect can be interpreted as a predominant growth of the small-scale turbulent magnetic field component with a little contribution of large-scale magnetic field amplification (see Otmianowska-Mazur et al. 2007 for a more extended analysis of the simulations presented in this section). One should remember, however, that numerical resistivity, always present in numerical MHD simulations, may influence to some extent the behavior of the simulation run A, corresponding to $\eta = 0$. The amount of numerical magnetic diffusivity $\eta \approx 0.7 \text{ pc}^2 \text{ Myr}^{-1}$ has been

quantified, for the present grid resolution, on the base of Parker instability simulations by Kowal et al (2003).

When magnetic diffusivity is increased up to $\eta = 100 \text{ pc}^2 \text{ Myr}^{-1}$ the efficiency of magnetic field amplification increases. For $\eta = 100 \text{ pc}^2 \text{ Myr}^{-1}$ (run A4) the growth of magnetic flux persists until $t = 1000 \text{ Myr}$ and saturates thereafter. For smaller values of η the growth rate is smaller and the maximum values of magnetic flux are smaller than those attained for $\eta = 100 \text{ pc}^2 \text{ Myr}^{-1}$. In cases of vanishing or small explicit diffusivity (runs A1 and A2), magnetic energy grows up initially faster than in the case of larger resistivity (runs A3 and A4). This behavior means that low resistivity enables initially faster growth of the random magnetic field component, while for larger resistivity random magnetic fields are quickly dissipated. The growth of the total magnetic energy follows closely, in the latter case, the growth of the mean magnetic flux. It is also apparent that amplification of magnetic flux and magnetic energy for $\eta = 1000 \text{ pc}^2 \text{ Myr}^{-1}$ (run A5) is significantly reduced with respect to the other runs.

In order to explain the physical mechanism that controls magnetic field amplification through the magnitude of magnetic diffusivity we plot the ratio of total (volume integrated) energies of vertical to azimuthal magnetic field components in Fig. 3. It is apparent that the energy of vertical magnetic field dominates in all lower magnetic diffusivity runs A1-A3 ($\eta = 0, 1$ and $10 \text{ pc}^2 \text{ Myr}^{-1}$) and is comparable to the energy of azimuthal magnetic field in run A4 ($\eta = 100 \text{ pc}^2 \text{ Myr}^{-1}$) providing the strongest magnetic field amplification. Among all simulations of series A only simulation A4 reaches energetic equipartition between magnetic field and gas kinetic energy as a result of the amplification process.

On the other hand, in the case of large magnetic diffusivity (run A5, $\eta = 1000 \text{ pc}^2 \text{ Myr}^{-1}$) energy of the vertical magnetic field component remains much smaller than energy of the azimuthal magnetic field and magnetic field amplification does not occur. This fact can be interpreted by resistive damping of the undulatory mode of the Parker instability in favor of the interchange mode, which does not contribute to the dynamo action. The above finding indicates that *the most favorable conditions for magnetic field amplification corresponds to approximately equal energies in vertical and azimuthal magnetic fields in the case of buoyancy driven dynamo.*

To demonstrate the effect of resistivity on kinetic and magnetic turbulent spectra we compute the Fourier transforms of kinetic and magnetic energy densities, as in the paper by Otmianowska-Mazur et al (2007). The results are shown in Fig 4. The highly anisotropic nature of turbulence is reflected by different lines representing Fourier transforms in x , y and z -directions. We find that the kinetic spectra, which are generally close to the Kolmogorov spectrum $\propto k^{-5/3}$, depend rather weakly on magnetic diffusivity. The large values of magnetic diffusivity $\eta = 100 \div 1000 \text{ pc}^2 \text{ Myr}^{-1}$ lead only to the damping of the short-wavelength components of the Fourier spectrum computed in y -direction.

The magnetic spectra appear to be much more sensitive to variations in magnetic diffusivity. The plots obtained for runs A1 and A2 exhibit practically identical spectra in all directions. This means that the diffusivity of $1 \text{ pc}^2 \text{ Myr}^{-1}$ does not change the results with vanishing explicit resistivity, or in other words the numerical resistivity of the code corresponds to the resistivity of Run A2. The effect of resistivity is apparent through the reduced amplitude of large- k modes for $\eta = 10 \text{ pc}^2 \text{ Myr}^{-1}$ (Run A3) and an apparent cutoff in magnetic spectra around $k/2\pi \approx 0.2 \text{ pc}^{-1}$ for $\eta = 100 \text{ pc}^2 \text{ Myr}^{-1}$. Further increase of magnetic diffusivity

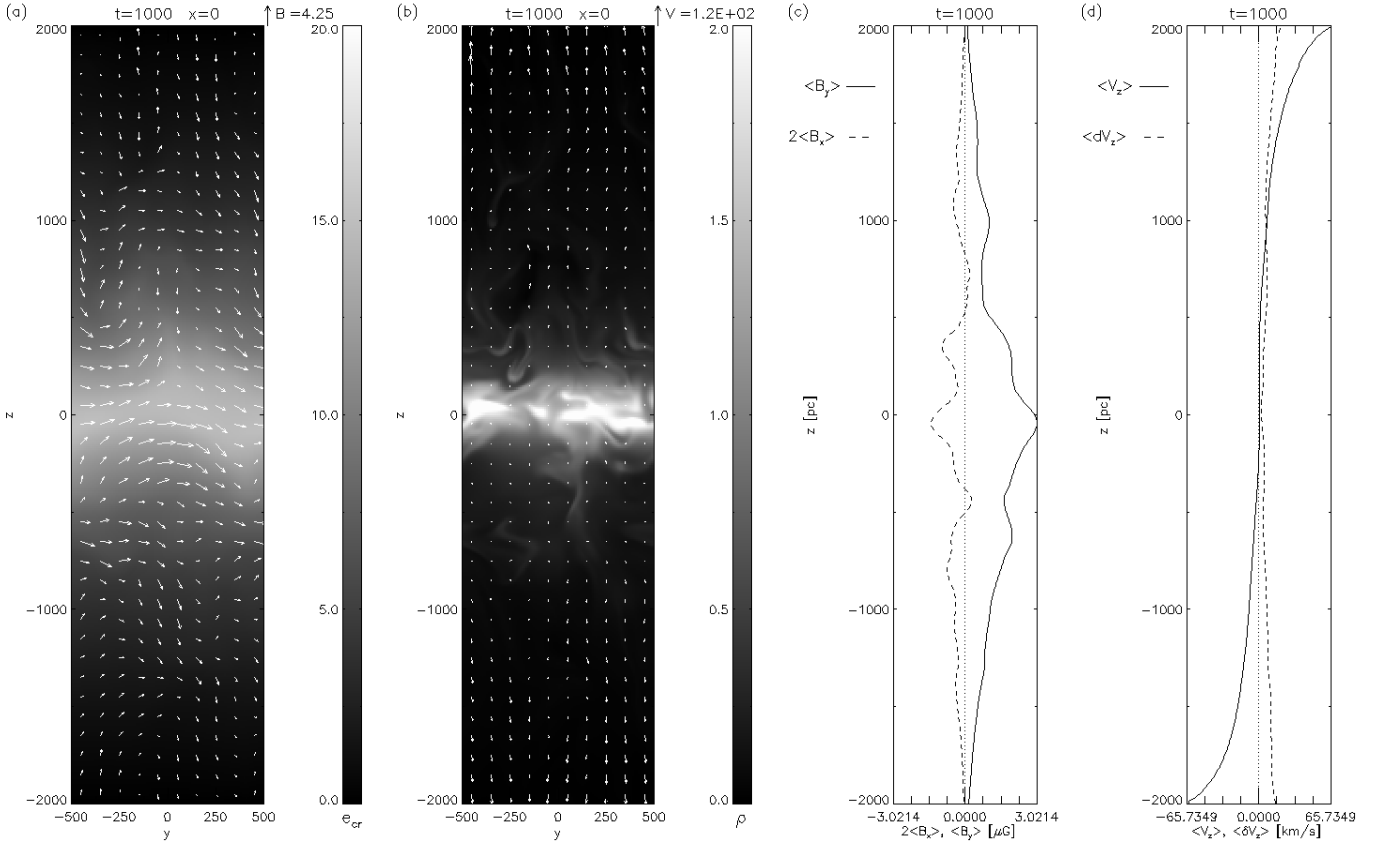


Fig. 1. Exemplary plots illustrating the state of the system at $t = 1000$ Myr for simulation A4. In the first two panels we present slices through the computational volume in the yz -plane for $x = 0$. Panel (a) shows cosmic ray energy density with vectors of magnetic field, panel (b) shows gas density with velocity vectors. In panel (c) we plot horizontally averaged x and y components of magnetic field, and in panel (d) horizontally averaged vertical velocity component and its fluctuations.

up to $\eta = 1000 \text{ pc}^2 \text{ Myr}^{-1}$ leads to the significant reduction of amplitudes of all modes for the Fourier transforms performed in z -direction, stepping of the whole spectrum in z -direction and a surprising effect of flattening of the spectrum in x -direction. The latter effect may indicate a qualitative change of the physical nature of the modes, which can plausibly be attributed to the mentioned enhancement of the exchange mode of Parker instability.

We briefly note that we neglect any small scale dynamics of the helical MHD turbulence. This assumption allows the uniformity of our diffusion coefficients, like the magnetic diffusivity. Detailed investigations of the influence of small scale helical MHD turbulence on galactic dynamos are presented by Maron & Blackman (2002) and Maron, Cowley and McWilliams (2004).

One can further interpret these results in terms of topological evolution of magnetic field which is controlled by resistivity. The topology of magnetic field lines determines the paths of anisotropic cosmic ray transport. For low values of resistivity the buoyancy of cosmic rays leads to opening of magnetic field lines through upper- and lower- z boundaries. This implies that diffusive escape of cosmic rays, along the open magnetic field lines, dominates over the buoyancy and limits the effect of Coriolis force, which is responsible for dynamo action.

4.2. The effect of spiral arms

In this section we describe the simulation series B performed for the same set of simulation parameters as for series A with an ex-

ception that currently the cosmic ray energy input is modulated in time by a step function. Motivation for this kind of CR supply is the presence of spiral arms in disk galaxies. We assume that SNe explode in arms with the rate, which is proportional to star formation rate. We assume that arms pass through the volume of our local computational domain once per 100 Myr and that the arm passage takes 25 Myr, i.e. starting at $t = 0$ we supply CRs for the first 25 Myr of the 100 Myr and stop CR supply for the remaining 75 Myr. We enhance the SN rate in arms 4 times, so that the average SN rate over the whole period of density wave remains the same as in the simulation series A. The evolution of mean magnetic flux and energy is presented in Fig. 5.

We find that in the present set of simulations, both magnetic flux and magnetic energy grow up faster than in the case of simulations without CR modulation. Magnetic field amplification is now apparent even in simulations with $\eta = 0$. The only exception is the $\eta = 1000 \text{ pc}^2 \text{ Myr}^{-1}$ simulation which does not show a noticeable amplification of magnetic field, even in the presence of CR modulation. This indicates that the temporal modulation of SN rate acts in the same way as increasing magnetic diffusivity in the range of $\eta = 0 \div 100 \text{ pc}^2 \text{ Myr}^{-1}$.

To interpret the above results we suggest the following scenario: CRs supplied to the system trigger Parker instability and leave the disk volume via combined buoyant and diffusive transport. Vertical magnetic loops form efficiently during the period of enhanced SN activity, but later on, in absence of CR perturbations, magnetic field tends to relax before the next spiral arm passage. In absence of CR forcing, in the inter-arm regions even a small resistivity is sufficient to relax magnetic field structure

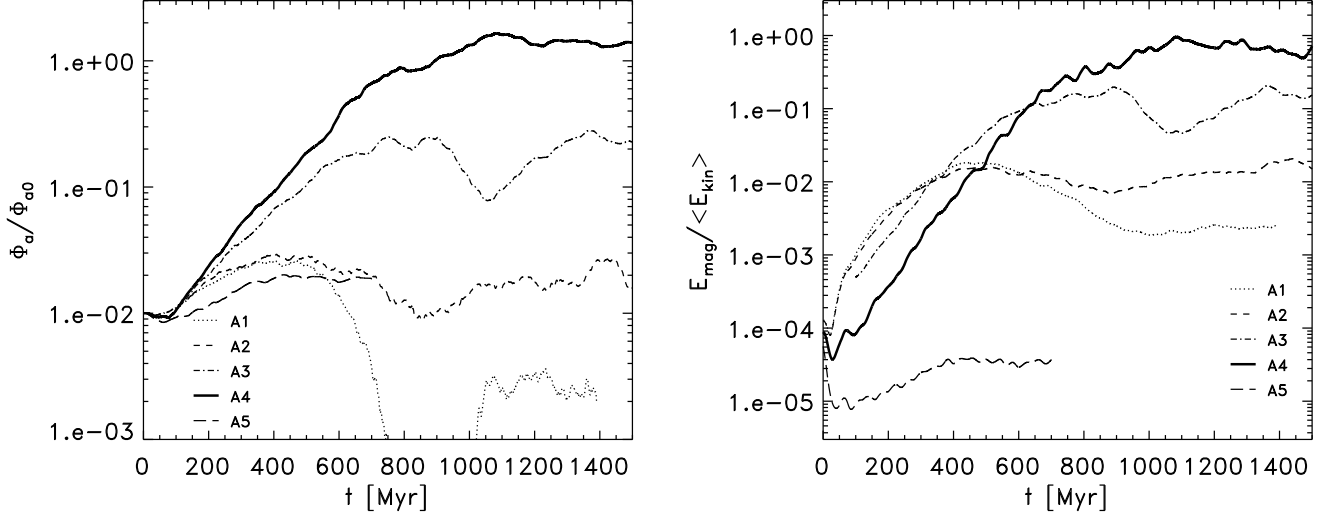


Fig. 2. Time evolution of azimuthal magnetic flux and total magnetic energy for different values of magnetic diffusivity in simulation series A. The curves represent respectively cases of $\eta = 0$ (A1), $\eta = 1$ (A2), $\eta = 10$ (A3), $\eta = 100$ (A4) and $\eta = 1000$ (A5) in units $\text{pc}^2 \text{Myr}^{-1}$.

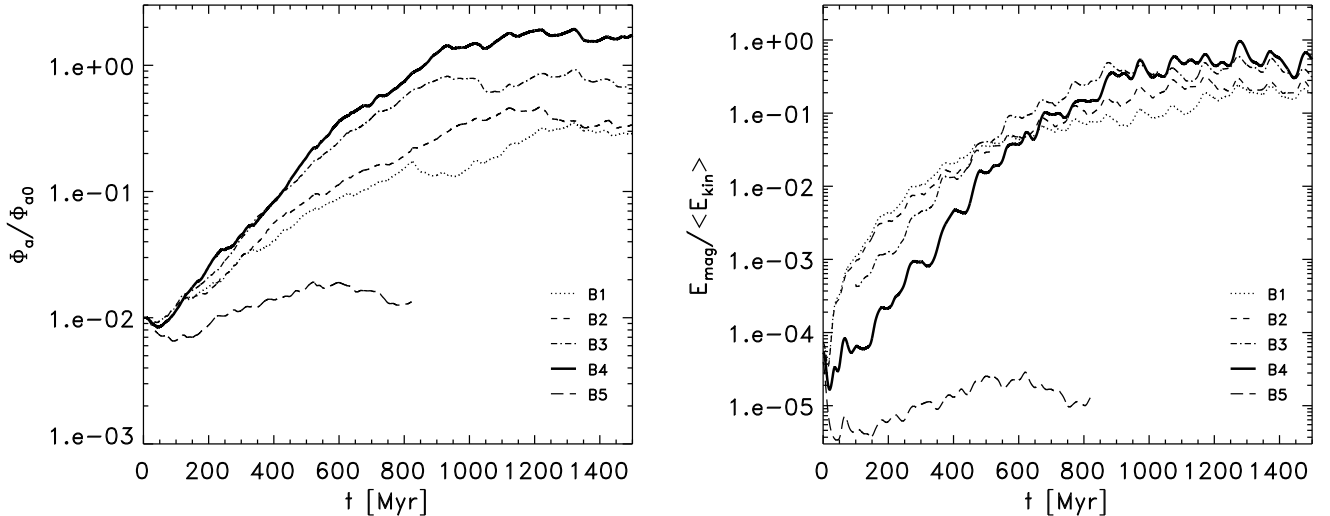


Fig. 5. Time evolution of azimuthal magnetic flux and total magnetic energy for different values of magnetic diffusivity, in presence of temporal modulations of SN-rate mimicking the presence of spiral arms in the simulation series B. The curves represent respectively cases of $\eta = 0$ (B1), $\eta = 1$ (B2), $\eta = 10$ (B3), $\eta = 100$ (B4) and $\eta = 1000$ (B5) in units $\text{pc}^2 \text{Myr}^{-1}$.

to the horizontal more regular configuration which suppresses excessive losses of CRs via the diffusive transport. Thus the efficiency of magnetic field amplification is enhanced.

4.3. Dependence of magnetic field amplification on SN-rate

In all runs of the simulation series A and B we adopted the fiducial value of $f_{SN} = 130 \text{kpc}^{-2} \text{Myr}^{-1}$ derived from the global model of Milky Way by Ferriere (1998) at galactocentric radius $R_G = 5 \text{kpc}$. In this section we describe simulation series C performed for different SN rates $f_{SN} =$

15, 30, 60, 250 and $500 \text{kpc}^{-2} \text{Myr}^{-1}$, together with run B4 ($f_{SN} = 130 \text{kpc}^{-2} \text{Myr}^{-1}$), to examine the effect of SN rate on magnetic field amplification. The results are shown in Fig. 6. In all cases the SN input is modulated in a manner described in Sect. 4.2.

One can notice that the magnetic field amplification rates and the final saturation levels of both magnetic flux and magnetic energy grow with f_{SN} as long as the SN rate is lower or equal to the fiducial, realistic value of $f_{SN} = 130 \text{kpc}^{-2} \text{Myr}^{-1}$ at galactocentric radius $R_G = 5 \text{kpc}$, when all other disk parameters are fixed. The e-folding times of magnetic flux deduced from the left panel

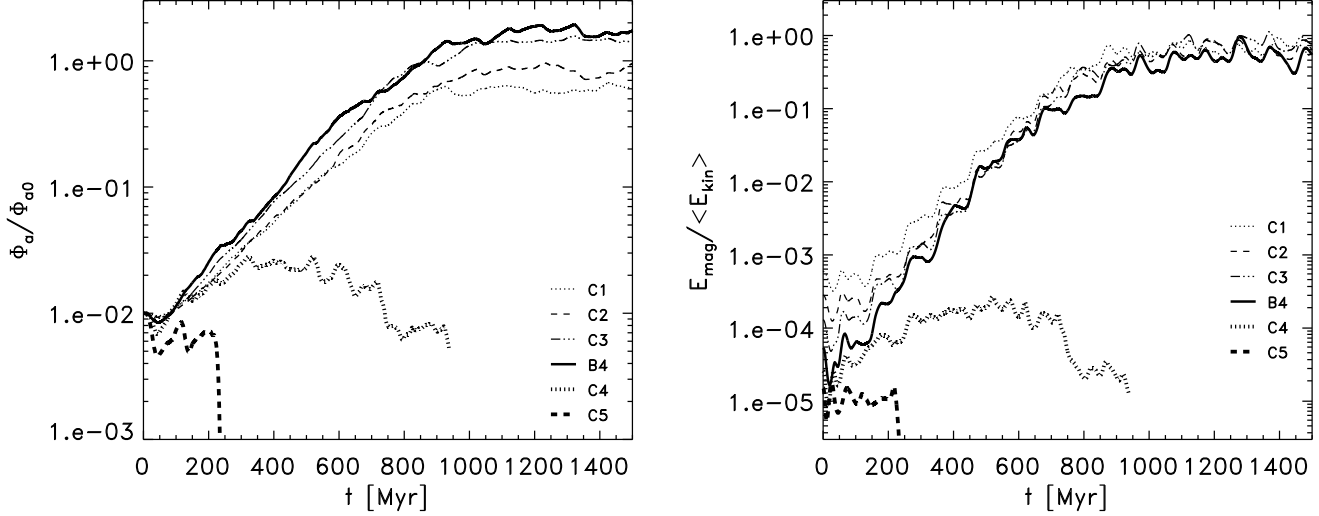


Fig. 6. Time evolution of azimuthal magnetic flux and total magnetic energy for different values of SN rate applied in simulation series C, together with run B4, in the presence of temporal modulations of SN-rate. Line assignments are respectively: $f_{SN} = 15$ (C1), $f_{SN} = 30$ (C2), $f_{SN} = 60$ (C3), $f_{SN} = 130$ (B4), $f_{SN} = 250$ (C4), and $f_{SN} = 500$ (C5) supernova explosions per squared kpc per Myr.

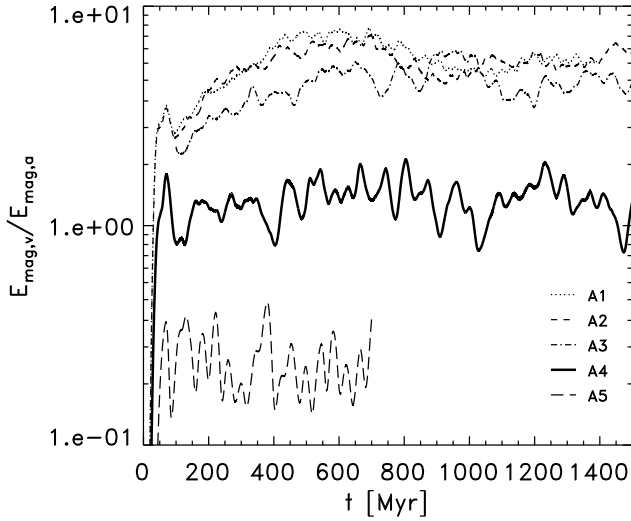


Fig. 3. Time evolution of the ratio of energies of vertical to horizontal magnetic field components for different values of magnetic diffusivity in the simulation series A. Line assignments are the same as in Fig. 2

of Fig. 6 are respectively 150 Myr for $f_{SN} = 130 \text{ kpc}^{-2} \text{ Myr}^{-1}$ (Run B4) and 190 Myr for $f_{SN} = 15 \text{ kpc}^{-2} \text{ Myr}^{-1}$ (Run C1). We note therefore that the magnetic field amplification rate is relatively insensitive to the magnitude of SN rate within the range of SN rates spanning one decade below the fiducial value. We note also that magnetic field amplification saturates at the level of equipartition of magnetic and kinetic energies in the case of

those simulation runs of series C for which the amplification holds.

When the SN rate is doubled, with respect to the fiducial value, then only a short period of magnetic field amplification is observed, until $t = 500$ Myr, and if SN rate is doubled once again then magnetic field decays. The above results show that magnetic field amplification holds in a wide range of SN rates and that the realistic values of SN rates are optimal for the galactic dynamo process. Similarly as in Sect. 4.1 we show the ratio of energies in vertical to horizontal magnetic field components in Fig. 7. We find that for SN rates up to $f_{SN} = 130 \text{ kpc}^{-2} \text{ Myr}^{-1}$ the efficient magnetic field amplification is associated with the ratio of vertical to horizontal magnetic field energies fluctuating around one, and in the case of excessive CR supply ($f_{SN} = 250 \text{ kpc}^{-2} \text{ Myr}^{-1}$ and more) the vertical magnetic field energy dominates and magnetic field ceases to grow.

4.4. Dependence of magnetic field amplification the grid resolution

In order to check the influence of the grid resolution on simulation results we increase the cell size to $(20 \text{ pc})^3$ in simulations D1 and D2 and apply the same parameters as in simulations A4 and B4, respectively. In Fig. 8 we show the evolution of the total flux of the azimuthal magnetic field component and the total magnetic energy for simulations D1 and D2 together with analogous curves for simulations A4 and B4, shown previously in Figs. 2 and 5. It is apparent that the results obtained at both resolutions are very similar, although a slightly faster growth of magnetic field is observed in simulations performed at the lower resolution, which can be explained by somewhat larger numerical resistivity.

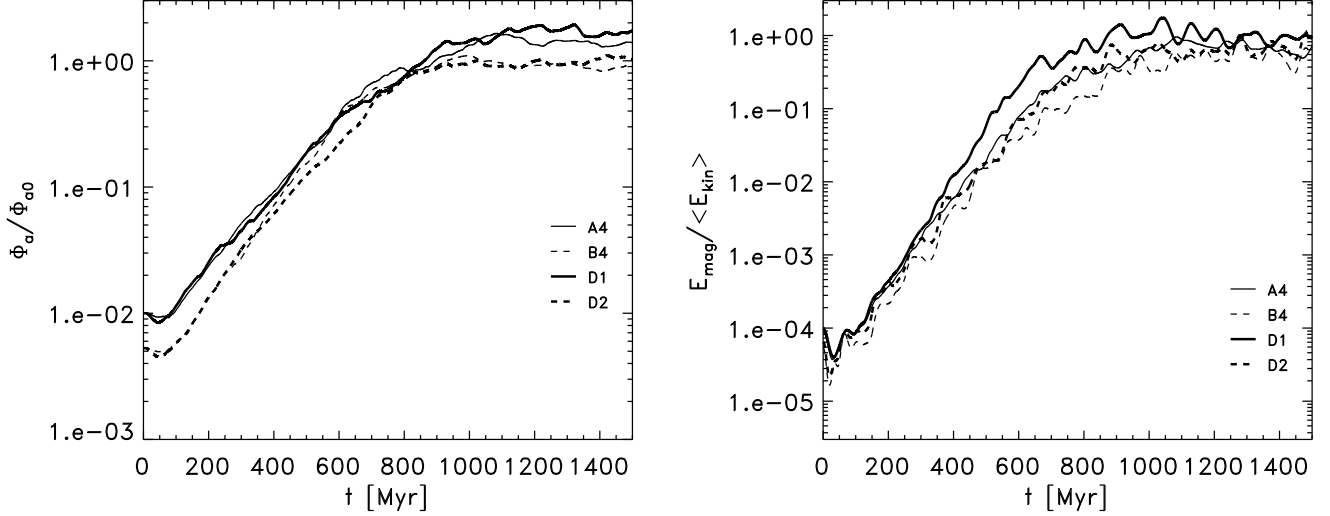


Fig. 8. Time evolution of the azimuthal magnetic flux and the total magnetic energy for simulations with grid resolutions $(10\text{pc})^3$ (runs A4 and B4) and $(20\text{pc})^3$ (runs D1 and D2).

4.5. Dependence of magnetic field amplification on CR diffusion coefficients

The aim of simulation series E is to examine the effect of variations of the CR diffusion coefficients on magnetic field amplification. All simulations of series E are performed with the resolution $(20\text{pc})^3$. The reduced grid resolution makes it possible to enlarge CR diffusion coefficients to realistic values, while preserving acceptable timesteps for the explicit integration algorithm of the CR diffusion-advection equation.

In the present simulation series E we vary parallel and perpendicular diffusion coefficients choosing different pairs from the set: $K_{\parallel} = 1 \times 10^4, 3 \times 10^4$ and $1 \times 10^5 \text{pc}^2 \text{Myr}^{-1}$, and $K_{\perp} = 1 \times 10^3, 3 \times 10^3$ and $1 \times 10^4 \text{pc}^2 \text{Myr}^{-1}$. The results of new simulations as compared to the run D1 are presented in Fig. 9.

The results of simulation series E can be summarized as follows. We note, that magnetic field growth rate and the saturation values of magnetic flux and energy depend particularly on the choice of K_{\parallel} and K_{\perp} . When K_{\parallel} is increased 3 and 10 times with respect to D1, the initial growth of magnetic field becomes slightly faster and the saturation level becomes lower by a factor of $2 \div 3$, provided that K_{\perp} is not too large. For $K_{\parallel} = 3 \times 10^4 \text{pc}^2 \text{Myr}^{-1}$ amplification holds for $K_{\perp} = 1 \times 10^3 \text{pc}^2 \text{Myr}^{-1}$ and $3 \times 10^3 \text{pc}^2 \text{Myr}^{-1}$, but for $K_{\perp} = 1 \times 10^4 \text{pc}^2 \text{Myr}^{-1}$ magnetic field decays. Similarly, for $K_{\parallel} = 1 \times 10^5 \text{pc}^2 \text{Myr}^{-1}$ amplification holds for $K_{\perp} = 1 \times 10^3 \text{pc}^2 \text{Myr}^{-1}$ and $K_{\perp} = 3 \times 10^3 \text{pc}^2 \text{Myr}^{-1}$, but for $K_{\perp} = 1 \times 10^4 \text{pc}^2 \text{Myr}^{-1}$ we find only initial growth until $t = 450 \text{Myr}$ and decay thereafter. The present results indicate that magnetic field amplification is possible only for $K_{\perp} \leq 3 \times 10^3 \text{pc}^2 \text{Myr}^{-1} \approx 10^{27} \text{cm}^2 \text{s}^{-1}$. Therefore the anisotropy of CR diffusion seems to be a crucial condition for magnetic field amplification in the process of the CR-driven dynamo.

In the subsequent Fig. 10 we show the energy ratio of vertical to azimuthal magnetic field components for runs E4, E5 and E6, corresponding to three different values of K_{\perp} and $K_{\parallel} = 1 \times 10^5 \text{pc}^2 \text{Myr}^{-1}$. Comparing Figs. 9 and 10 we find that in the case of two simulation runs E4 and E5 (two smaller values of K_{\perp}) the energy ratio of vertical to azimuthal magnetic field com-

ponents varies in the range $\sim 0.3 \div 2$, corresponding to efficient growth magnetic energy. For the largest value of $K_{\perp} = 10^4$ the magnetic energy ratio becomes occasionally larger by an order of magnitude, magnetic field decays.

4.6. The issue of energy equipartition

The results presented so far demonstrate that magnetic fields amplified by the CR-driven dynamo saturate near equipartition of magnetic and gas kinetic energies. It is commonly expected that CRs remain in energetic equipartition with gas and magnetic field as well.

To investigate the relation of CR to other forms of energies, we plot in Fig. 11 the time evolution of the ratio of CR to the time-averaged turbulent kinetic energy (we subtract the kinetic energy of the large-scale shear flow) for different values of CR diffusion coefficients (the simulation series E). We find that, depending on diffusion coefficients, CR energy is larger than the turbulent kinetic energy by a factor of 10 – 50, while the magnetic field energy, according to the results presented in Fig. 9, is close to the gas turbulent energy.

It is apparent that for the first few hundred Myr CRs accumulate quickly in the disk since they are trapped by horizontal magnetic field. The ratio of CR to kinetic energies saturates as soon as vertical magnetic field component appears, due to buoyancy, enabling diffusive transport of CRs out of the disk.

When the cosmic ray diffusion coefficients are larger, one can find that the ratio of CR to kinetic energies is lower. We note, that cosmic rays find an easier way to leave the disk, when the parallel and perpendicular diffusion coefficients are larger. The results shown in Fig. 11 indicate that the ratio of CR to kinetic energies anticorrelates with both: the parallel and perpendicular CR diffusion coefficients. Due to the mentioned timestep limitation, in the simulations presented in this paper we could only adopt the values of K_{\parallel} reaching at most $3 \times 10^{28} \text{cm}^2 \text{s}^{-1}$, that are still smaller than $10^{29} \text{cm}^2 \text{s}^{-1}$ mentioned by other authors (e.g. Jokipii 1999). Although the tendency of lowering the CR energy with the magnitude of the parallel CR diffusion coefficient

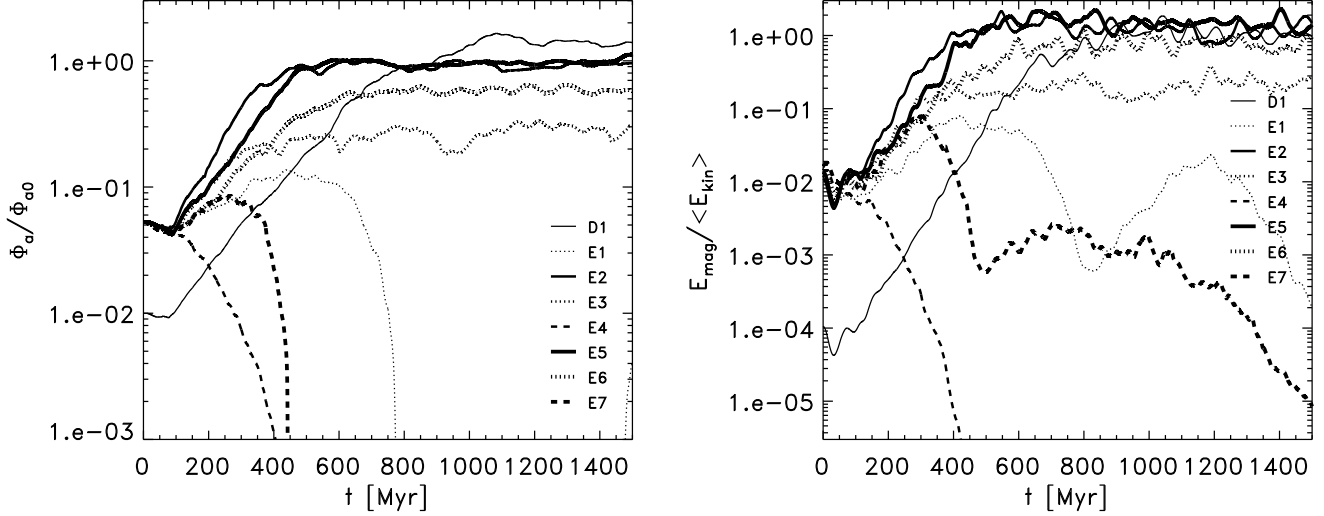


Fig. 9. Time evolution of the azimuthal magnetic flux and the total magnetic energy for different values of the parallel and perpendicular CR diffusion coefficients. Thin lines are used for $K_{\parallel} = 1 \times 10^4$ (runs D1 and E1), mid lines are used for $K_{\parallel} = 3 \times 10^4$ (runs E2 E3 and E4) and thick lines are used for $K_{\parallel} = 1 \times 10^5$ (runs E5 E6 and E7). Full lines denote $K_{\perp} = 1 \times 10^3$ (runs D1, E2 and E5), dotted lines denote $K_{\perp} = 3 \times 10^3$ (runs E1, E3 and E6), dashed lines $K_{\perp} = 1 \times 10^4$ (runs E4 and E7). All diffusion coefficients given in units $\text{pc}^2 \text{Myr}^{-1}$.

seems promising, one should not expect that values as large as $K_{\parallel} \approx 10^{29} \text{cm}^2 \text{s}^{-1}$ will reduce the problem of CR energy excess.

Another factor, which may significantly influence the relation between CR and other form of energies, is the choice of periodic and shear-periodic boundary conditions in the horizontal directions of the computational box. In real galactic disks, CR diffusion is expected along horizontal magnetic field lines. In the case of periodic-type boundary conditions, CRs are trapped in the disk volume by predominantly horizontal magnetic field. This kind of trapping can be released, however, only in the global galactic disk simulations.

5. Summary and conclusions

In the present paper we described an extensive series of simulations and presented parameter study of the CR-driven dynamo in a galaxy, characterized by the essential parameters typical for the Milky Way at galactocentric radius $R_G = 5 \text{kpc}$. In the presented study the magnetic diffusivity, as well as the parallel and perpendicular CR diffusion coefficients have been considered as free parameters, and dedicated simulation series have been performed to investigate their influence on the efficiency of the CR-driven dynamo process. The results of the parameter study can be summarized as follows:

(1) The magnitude of magnetic diffusivity influences essentially the efficiency of magnetic field amplification. The most favorable value of magnetic diffusivity is $100 \text{pc}^2 \text{Myr}^{-1} \approx 3 \times 10^{25} \text{cm}^2 \text{s}^{-1}$, the value comparable, although lower than the the value of turbulent diffusivity of ISM deduced from observational data.

(2) The efficiency of magnetic field amplification is enhanced by temporal modulation of the CR supply. An effect of this kind may be associated with the periodicity of star formation and supernova activity induced by spiral arms. The enhancement

is apparent at lower values of magnetic diffusivity and is less significant at the optimal value of $\eta = 100 \text{pc}^2 \text{Myr}^{-1}$.

(3) Magnetic field amplification rate is relatively insensitive to the magnitude of SN rate within the range of SN rates spanning one decade below the value $f_{SN} = 130 \text{kpc}^{-2} \text{Myr}^{-1}$ typical for galactocentric radius $R_G = 5 \text{kpc}$. We note also that magnetic field amplification saturates at the level of equipartition of magnetic and kinetic energies for all supernova rates for which amplification holds. Magnetic field is no longer amplified, if SN rate is further enhanced by factors 2 and 4 with respect to the realistic value, while other quantities (like e.g. gas column density) remain fixed.

(4) Magnetic field amplification in the CR-driven dynamo relies on anisotropic diffusion of cosmic rays. From the limited set of simulations of series E, one can deduce that the magnetic field amplification is possible only for $K_{\perp} \leq 3 \times 10^3 \text{pc}^2 \text{Myr}^{-1} \approx 10^{27} \text{cm}^2 \text{s}^{-1}$, and for all considered values of the parallel diffusion coefficient K_{\parallel} in the range $3 \div 30 \times 10^{27} \text{cm}^2 \text{s}^{-1}$. Therefore, the 5% ratio of the perpendicular to parallel diffusion coefficients postulated by Giacalone & Jokipii (1998) falls within the amplification range.

(5) By varying various parameters: magnetic diffusivity, supernova rate and the CR diffusion coefficients, we have found that the favorable conditions for magnetic field amplification correspond to approximately equal energies of the vertical and azimuthal magnetic field components in the case of buoyancy driven dynamo. An excess or deficit of vertical magnetic field with respect to the azimuthal one corresponds to significantly less efficient amplification or even decay of magnetic field.

(6) We note the problem indicated previously by Snodin et al (2005), that in all simulations the CR energy in the computational domain exceeds the turbulent kinetic energy and magnetic energy by more than one order of magnitudes. Moreover, the lowest ratios of CR to kinetic energies emerge for the largest values of the parallel diffusion coefficient. It seems not plausi-

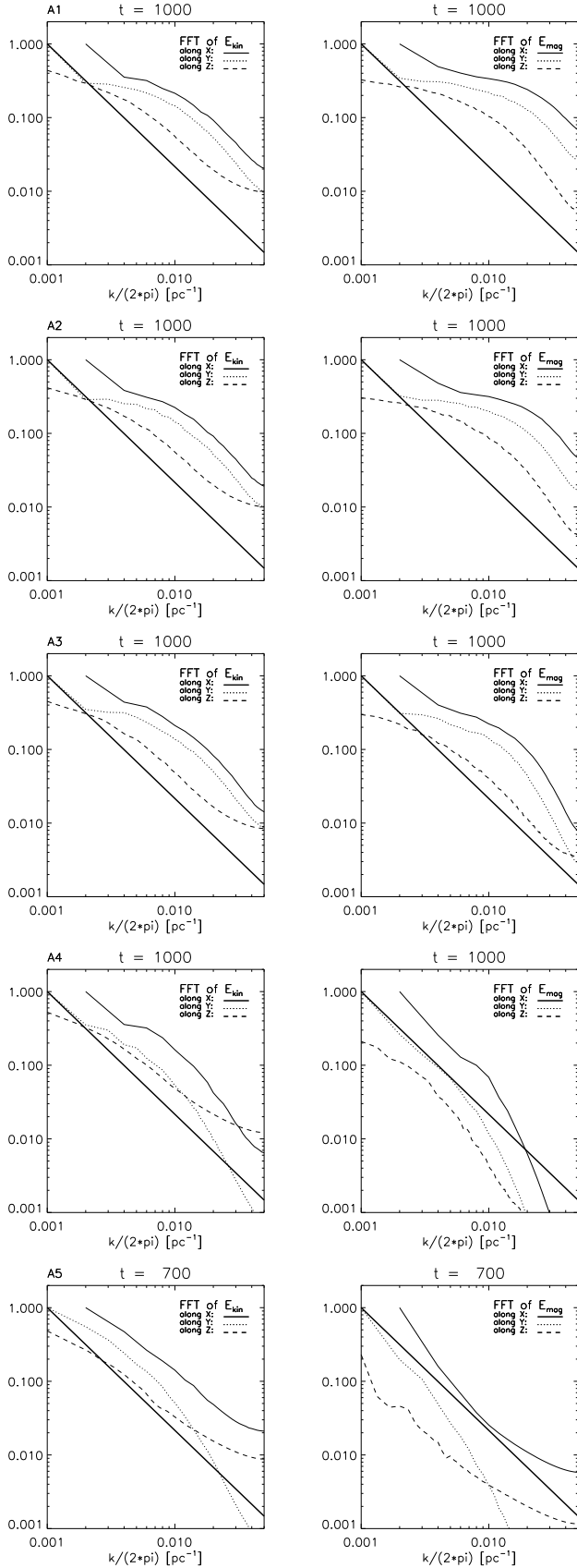


Fig. 4. Kinetic (left column) and magnetic (right column) spectra computed for $t = 1000$ Myr (runs A1-A4) and $t = 700$ Myr (Run A5), separately in x , y and z -directions (full, dotted and dashed thin lines, respectively). Lines representing the $k^{-5/3}$ slope (thick full lines) are shown for comparison.

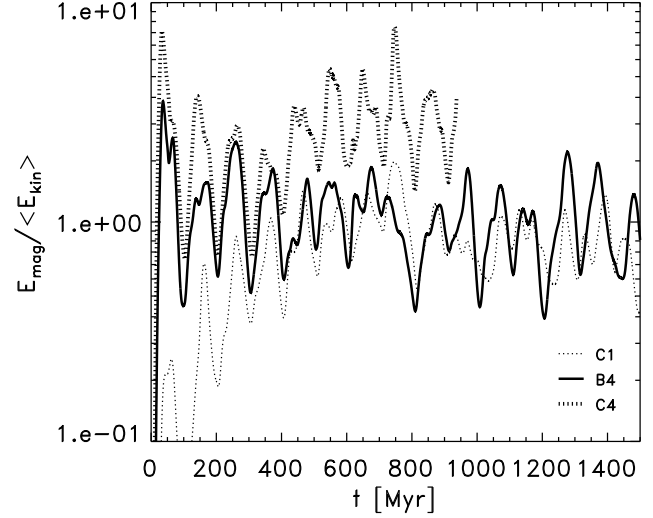


Fig. 7. Time evolution of the ratio of energies of vertical to horizontal magnetic field components for different (modulated) SN rates $f_{SN} = 15$ (C1), $f_{SN} = 130$ (B4) and $f_{SN} = 250$ (C4) supernova explosions per squared kpc per Myr.

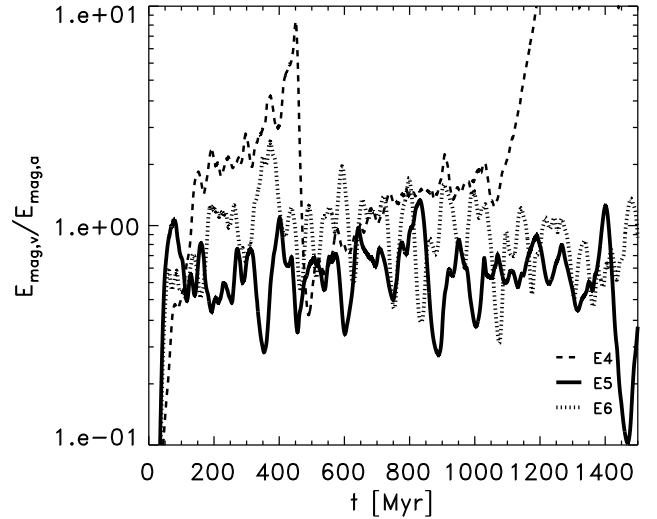


Fig. 10. Time evolution of the ratio of energies of vertical to horizontal magnetic field components for different values of the perpendicular CR diffusion coefficients $K_{\parallel} = 3 \times 10^4$ and $K_{\perp} = 1 \times 10^4$ (E4), $K_{\parallel} = 1 \times 10^5$ and $K_{\perp} = 1 \times 10^3$ (E5) and $K_{\parallel} = 1 \times 10^5$, $K_{\perp} = 3 \times 10^3$ (E6). All diffusion coefficients given in units $\text{pc}^2 \text{Myr}^{-1}$.

ble, however, that an enlargement of diffusion coefficients up to fully realistic values will reduce the excess of cosmic rays energy in the disk. It seems also, that the ratio of CR to other forms of energy in the ISM is not yet well restricted on observational grounds (Strong et al 2007). On the other hand, the currently used shearing box approximation does not permit CRs to leave the disk by means of diffusion along the predominantly horizon-

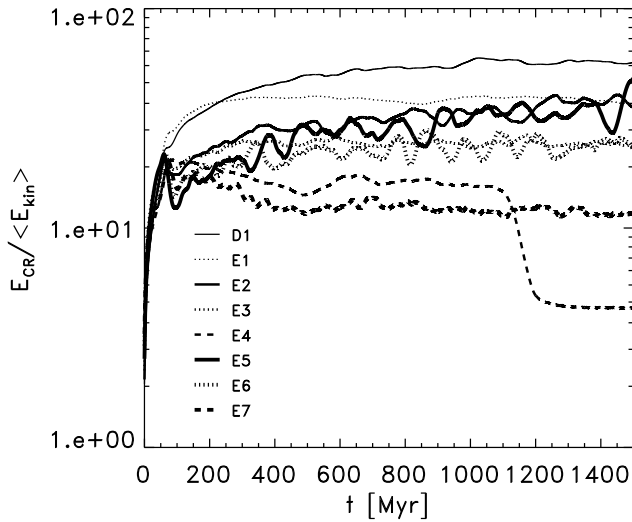


Fig. 11. Time evolution of the ratio of CR to time-averaged kinetic energy for different values CR diffusion coefficients in simulation series E. Line assignments are the same as in Fig. 9

tal magnetic field. Therefore, we suggest that subsequent work on the CR-driven dynamo, aimed to solve this problem, should be done in the framework of global galactic disk simulations.

Acknowledgements. This work was supported from the Polish Committee for Scientific Research (KBN) through the grants PB 0656/P03D/2004/26 and 2693/H03/2006/31.

References

Beck R., 2007, arXiv:0711.4700
 Beck, R, Krause, M., 2005, *Astronomische Nachrichten* 326
 Berezhinskii, V.S., Bulanov, S.V., Dogiel, V.A., Ginzburg, V.L., Ptuskin, V.S., *Astrophysics of cosmic rays*, Amsterdam: North-Holland, 1990.
 Chi, X., Wolfendale, A.W., *Nature* 362, 610 (1993)
 Ferriere, K. 1998, *ApJ*, 497, 759
 Fitt, A.J., Alexander, P., *MNRAS*, 261, 445 (1993)
 Giacalone, J., Jokipii, R.J., 1999, *ApJ*, 520, 204
 Gressel, O., Ziegler, U., Elstner, D., Rüdiger, G. 2008, *AN*, 329, 61
 Gressel, O., Elstner, D., Ziegler, U., Rüdiger, G. 2008, *A&A*, 486L, 35
 Hanasz, M., Lesch, H. 1993, *A&A*, 278, 561
 Hanasz, M., Lesch, H. 1997, *A&A*, 321, 1007
 Hanasz, M., Lesch, H. 1998, *A&A*, 332, 77
 Hanasz, M. Lesch, H. 2000, *ApJ*, 543, 235
 Hanasz, M. Lesch, H. 2001, *Space Sci. Rev.*, 99, 231.
 Hanasz, M., Otmianowska-Mazur, K., Lesch, H. 2002, *A&A*, 386, 347
 Hanasz, M., Lesch, H. 2003a, *A&A*, 404, 389
 Hanasz, M., Lesch, H. 2003b, *A&A*, 412, 331
 Hanasz, M., Kowal, G., Otmianowska-Mazur, K., & Lesch, H. 2004, *ApJ* 605, L33
 Hanasz, M., Kowal, G., Otmianowska-Mazur, K., & Lesch, H. 2006, *AN* 327, 469
 Hawley, J.F., Gammie, C.F., Balbus, S.A. 1995, *ApJ*, 440, 442
 Hessen, V., Dettmar, R.-J., Krause, M., Beck R., 2008, arXiv:0801.3542
 Jokipii, J.R.: 1999, in J. Franco and A. Carraminana (eds.) *Interstellar Turbulence*, Cambridge University Press, 70-78.
 Kowal, G., Hanasz, M., Otmianowska-Mazur, K., 2003, *A&A*, 404, 533
 Kowal, G., Otmianowska-Mazur, K., Hanasz, M., 2005, *A&A*, in press
 Lesch, H., Hanasz, M. 2003, *A&A*, 401, 809
 Maron, J., Blackman, E.G. 2002, *ApJ*, 566, L41
 Maron, J., Cowley, S., McWilliams, J. 2004, *ApJ*, 603, 569
 Otmianowska-Mazur, K., 2003, *A&A*, 408, 817
 Otmianowska-Mazur, K., Kowal, G., Hanasz, M., 2007, *ApJ*, 668, 1100
 Parker, E.N. 1992, *ApJ*, 401, 137

Ryu, D., Kim, J., Hong, S.S., Jones, T.W. 2003, *ApJ*, 589, 338
 Schlickeiser, R., Lerche, I. 1985, *A&A*, 151, 151
 Snodin, A. P., Brandenburg, A., Mee, A. J., Shukurov, A. 2005, astro-ph/0507176
 Stone, J.M., Norman, M.L., 1992a, *ApJS*, 80, 753
 Stone, J.M., Norman, M.L., 1992b, *ApJS*, 80, 791
 Strong, A.W., Moskalenko, I.V., Ptuskin, V.S., 2007, *Annual Review of Nuclear and Particle Systems*, 57, 285
 Tanuma, S., Yokoyama, T., Kudoh, T., Shibata, K. 2003, *ApJ*, 582, 215
 Vallee, J.P., *A&A*, 296, 819 (1995)